ィークロマトグラフィーによる精製を行った(図6)。

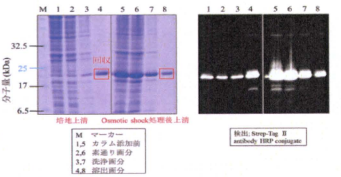

図 6　Strep-Tactin Sepharose による pepB 融合抗 EGFR VHH の精製後の SDS-PAGE, ウエスタンブロッティング結果

図6より、SDS-PAGEによって単バンドを確認できるまで精製されていることが分かり、このVHH断片をクラスター化の実験に使用した。

・クラスター化と機能評価

pepB融合VHH断片をそれぞれFITCで標識した後に、pepA融合フェリチンとpepB融合抗EGFR VHHを1対7の濃度で混合し、金属イオンとしてNi^{2+}イオンを加えることによって、FITC標識抗EGFR VHH断片をフェリチン分子表面にクラスター化させた。そして、抗原であるEGFRを発現しているヒト扁平上皮がん細胞A431に対する結合の様子を蛍光顕微鏡で観察した(図7)。フェリチンとN^{2+}を加えず、FITC標識抗EGFR VHH断片単独でA431細胞と相互作用させた結果と比較すると、VHH断片のみでは抗体濃度が減少していくにつれてその蛍光強度が低下していくのに対し(図7A)、VHH標識フェリボディーの場合では抗体濃度が減少しても、ほぼ一定の蛍光強度が得られたことが示された(図7B)。

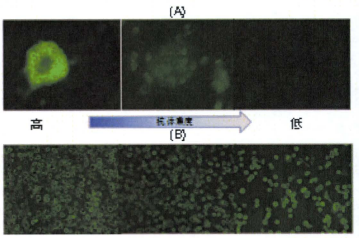

図 7　A431 細胞上の EGFR に対するイメージング評価
(A) pepB 融合 VHH-FITC 単独
(B) VHH 標識フェリボディー

D．考察

図7の結果から、このことからフェリチンを核として多価化することでより多くの抗原と結合できることが示唆され、このフェリボディーは低濃度でも検出可能なためイメージングに有用であることが言えた。

ラクダ抗体は、ヒト由来抗体と異なり、抗原結合部位が二量体ではなく単量体である。さらに、C末端が抗原認識領域の反対側にあるため、抗原結合機能を阻害することなく、様々なペプチド・蛋白質を融合すること可能である。本研究で用いたクラスター化デザインは、低分子抗体のクラスター化による多価効果が確認された。これより、ラクダ抗体は、タンパク質カプセル表

層に提示に適した低分子抗体であると言える。

E. 結論

本研究ではフェリチンをタンパク質カプセルとして、ラクダ抗体の抗原認識部位のみからなる低分子抗体を、活性を落とすことなくクラスター化させることに成功した。本研究より、ラクダ抗体由来の抗原認識ドメインがタンパク質カプセル表層に提示に適した低分子抗体であることが分かった。

F. 研究発表

1. 論文発表

1. Takanari Togashi, "One-pot Hydrothermal Synthesis of an Assembly of Magnetite Nanoneedles on a Scaffold of Cyclic-diphenylalanine Nanorods", Journal of Nanoparticle Research, in press.

2. Do-Myoung Kim, Mitsuo Umetsu, Kyo Takai, Takashi Matsuyama, Nobuhiro Ishida, Haruo Takahashi, Ryutaro Asano, and Izumi Kumagai, "Enhancement of cellulolytic enzyme activity by clustering of cellulose binding domain on nanoscaffolds", Small, 7, 656-664 (2011)

3. Takanari Togashi, Nozomi Yokoo, Mitsuo Umetsu, Satoshi Ohara, Takashi Naka, Seiichi Takami, Hiroya Abe, Izumi Kumagai, and Tadafumi Adschiri, "Material-binding peptide application -ZnO crystal structure control by means of a ZnO-binding peptide-", Journal of Bioscience and Bioengineering, 111, 140-145 (2011)

4. Mitsuo Umetsu, Takeshi Nakanishi, Ryutaro Asano, Takamitsu Hattori, and Izumi Kumagai, "Protein-protein interactions and selection: generation of molecule-binding proteins on the basis of tertiary structural information", FEBS Journal, 277, 2006-2014 (2010).

2. 学会発表

1. 植田 朝美, 階上 健太郎, 中西 猛, 浅野 竜太郎, 梅津 光央, 熊谷 泉, "低分子抗体の多機能化を目指したピンポイント化学接合デザイン", バイオ関連化学シンポジウム要旨集, 2A-12, (2010)

2. 植田 朝美, 階上 健太郎, 中西 猛, 浅野 竜太郎, 梅津 光央, 熊谷 泉, "低分子抗体の多機能化を目指したピンポイント化学接合デザイン", 第33回日本分子生物学会年会・第83回日本生化学会大会合同大会講演予稿集, 1P-1257 (2010)

G. 知的所有権の取得状況

1. 特許取得

特になし

2. 実用新案登録

特になし

3. その他

特になし

別紙４

研究成果の刊行に関する一覧表

書籍

著者氏名	論文タイトル名	書籍全体の編集者名	書　籍　名	出版社名	出版地	出版年	ページ
佐々木良平、丹生健一（共同編集）、鈴木志津枝－（編		佐々木良平、丹生健一	カラーアトラス　放射線療法・放射	日本看護協会出版会	東京	2011	
[分担執筆]佐々木良平、宮脇大輔	下垂体腫瘍	監修：唐澤克之他	タイトル：がん放射線療法・2010	篠原出版	東京	2010	625-632
[分担執筆]佐々木良平、宮脇大輔	別冊　下垂体腫瘍	監修：唐澤克之他	タイトル：がん放射線療法・2010	篠原出版	東京	2010	18-19
[分担執筆]佐々木　良平	放射線療法	監修：丹生健一他	耳鼻咽喉科・頭頚部外科研修ノート	診断と治療社	東京	2010	434-438

雑誌

発表者氏名	論文タイトル名	発表誌名	巻号	ページ	出版年
Matsui, K., Karasaki, M., Segawa, M., Hwang, S. Y., Tanaka, T., Ogino, C., Kondo, A	Biofunctional TiO_2 nanoparticle mediated photokilling of cancer cells using UV irradiation	MedChemComm	1	209-211	2010
Miyachi, Y., Shimizu, N., Ogino, C., Kondo, A	Selection of DNA aptamers using atomic force microscopy	*Nucleic Acids Research*	38	e21	2010

Fukuda, N., Ishii, J., Tanaka, T., Kondo, A	The competitor-introduced Gγrecruitment system, a new approach for screening affinity-enhanced proteins	FEBS Journal	277	1704-1712	2010
Kondo, A.	Protein-protein interactions and selection	FEBS Journal	277	1981	2010
Ishii, J., Fukuda, N., Tanaka, T., Ogino, C., Kondo, A	Protein-protein interactions and selection: yeast-based approaches that exploit guanine nucleotide-binding protein signaling	FEBS Journal	277	1982-1995	2010
Shimizu, N., Ninomiya, K., Ogino, C., M. M. Rahman	Potential uses of titanium dioxide in conjunction with ultrasound for improved disinfection	Biochemical Engineering Journal	48	416	2010
Ogino, C., Shibata, N., Sasai, R., Takaki, K., Miyachi, Y., Kuroda, S., Ninomiya, K., Shimizu, N	Construction of protein-modified Ti02 nanoparticles for use with ultrasound irradiation in a novel cell-injuring method	Bioorganic & Medicinal Chemistry Letters	20	5320-5325	2010
Shishido, T., Mieda, H., Hwang, S. Y., Nishimura, Y., Tanaka, T., Ogino, T., Fukuda, H., Kondo, A	Affibody-displaying bionanocapsules for specific drug delivery to HER2 expressing cancer cells	Bioorganic & Medicinal Chemistry Letters	20	5726-5731	2010

Komatsu, S., Fukumoto, T., Demizu, Y., Miyawaki, D., Terashima, K., Sasaki, R., Hori, Y., Hishikawa, Y., Yonson Ku, Y., Murakami, M.	Clinical results and risk factors of proton and carbon ion therapy for hepatocellular carcinoma	Cancer		in press	2011
Sasaki, R., Yasuda, K., Abe, E., Uchida, N., Kawashima,M., Uno, T., Fujiwara, M., Shioyama, Y., Kagami, Y., Shibamoto, Y., Nakata, K., Takada, Y., Kawabe, T., Uehara, K., Nibu, K., Yamada, S.	Multi-institutional Analysis of Solitary Extramedullary Plasmacytoma of the Head and Neck Treated with Curative Radiotherapy	Int J Radiat Oncol Biol Phys		in press	2011
Yoshida K, Sasaki R, Nishimura H, Miyawaki D, Kawabe T, Okamoto Y, Nakabayashi K, Yoshida S, Sugimura K	Radiotherapy for Japanese elderly patients with cervical cancer: preliminary survival outcomes and evaluation of treatment-related toxicity	Arch Gynecol Obstet		in press	2011
Wakahashi K, Shimoyama M, Katayama Y, Minagawa K, Yoshida K, Sasaki R, Nakayama S, Yokozaki H, Yanagita E, Itoh T, Hayashi Y, Matsui T	Histiocytic sarcoma with two immunohistopathologicall y distinct populations	Int J Hematol		in press	2011
Ikushima H, Dong L, Erasmus J, Allen P, McAleer MF, Zhuange Y, Sasaki R, Komaki R.	Predictive Value of (18)F-Fluorodeoxyglucos e Uptake by Positron Emission Tomography for Non-Small Cell Lung	J Radiat Res.		in press	2011

Mukubou H, Tujimura T, Sasaki R,Yonson Ku,	The role of autophagy in the treatment of pancreatic cancer with gemcitabine and ionizing radiation.	International Journal of Oncology	37	821-828	2010
Amalia H, Sasaki R, Suzuki Y, Demizu Y, Bito T, Nishimura H, Okamoto Y, Yoshida K, Miyawaki D, Kawabe T, Mizushina Y, and Kazuro S	Vitamin K2-derived Compounds Induce Growth Inhibition in Radioresistant Cancer Cells	Kobe J Med Sci	56	38-49	2010
Kumamoto-Yonezawa, Y., Sasaki, R., Suzuki, Y., Matsui, Y., Hada, T., Uryu, K., Sugimura, K., Yoshida, H., Mizushina, Y.	Enhancement of human cancer cell radiosensitivity by conjugated eicosapentaenoic acid - a mammalian DNA polymerase inhibitor	International Journal of Oncology	36	577-584	2010
Yoshida, K., Sasaki, R., Nishimura, H., Okamoto, Y., Suzuki, Y., Saitoh, M., Otsuki, N., Hayashi, Y., Soejima, T., Nibu, K., Sugimura, K.	Nuclear Factor-kappa B Expression as a Novel Marker of Radioresistance: In Early Stage Laryngeal	Cancer, Head Neck	32	646-655	2010
佐々木良平，橋本直樹，赤坂浩亮	放射線治療の有害事象	プロフェッショナルがんナーシング	1	63-73	2011
佐々木良平，西村英輝，椋本成俊	がん放射線治療の基礎知識	プロフェッショナルがんナーシング	1	42-55	2011

佐々木良平	PET診断と放射線治療	PET Journal	10	13-15	2010
D. Rangappa, T. Naka, S. Ohara, and T. Adschiri	Preparation of Ba-Hexaferrite Nanocrystals by an Organic Ligand-Assisted Supercritical Water	Crystal Growth & Design	10	11-15	2010
T. Mousavand, S. Ohara, T. Naka, M. Umetsu, S. Takami, and T. Adschiri	Organic-Ligand-Assisted Hydrothermal Synthesis of Ultrafine and Hydrophobic ZnO Nanoparticles	J. Mater. Res.	25	219-223	2010
K. Sato, H. Abe, and S. Ohara	Selective Growth of Monoclinic and Tetragonal Zirconia Nanocrystals	J. Am. Chem. Soc.	132	2538-2539	2010
T. Sasaki, S. Ohara, T. Naka, J. Vejpravova, V. Sechovsky, M. Umetsu, S. Takami, B. Jeyadevan, and T. Adschiri	Continuous Synthesis of Fine $MgFe_2O_4$ Nanoparticles by Supercritical Hydrothermal Reaction	J. Supercrit. Fluids	53	92-94	2010
Z. Tan, H. Abe, M. Naito, and S. Ohara	Arrangement of Palladium Nanoparticles Templated by Supramolecular Self-assembly of SDS Wrapped on Single-Walled Carbon Nanotubes	Chem. Comm.	46	4363-4365	2010
Z. Tan, H. Abe, M. Naito, and S. Ohara	Oriented Growth Behavior of Ag Nanoparticles using SDS as a Shape Director	J. Colloid Interface Sci.	348	289-292	2010

J. Zhang, H. Kumagai, K. Yamamura, S. Ohara, S. Takami, A. Morikawa, H. Shinjoh, K. Kaneko, T. Adschiri, and A. Suda	Extra-Low Temperature Oxygen Storage Capacity of CeO_2 Nanocrystals with Cubic Facets	Nano Lett.	11	361-364	2011
K. Sato, H. Abe, S. Ohara	Selective growth of Monoclinic and Tetragonal Zirconia Nanocrystals	Journal of the American Chemical Society	132	2538-2539	2010
K. Sato, T. Kinoshita, H. Abe	Performance and Durability of Nanostructured LSM/YSZ Cathode for Intermediate Temperature Solid Oxide Fuel Cells	Journal of Power Sources	195	4114-4118	2010
K. Sato, T. Kinoshita, H. Abe	Fine-microstructure Mediated Efficient Hydrogen Oxidation in Ni/YSZ Anode Fabricated from Novel Co-precipitation Derived Nanocomposites	Fuel Cells	10	320-324	2010
T. Togashi, T. Naka, S. Asahina, K. Sato, S. Takami, T. Adschiri	Surfactant-assisted one-pot synthesis of superparamagnetic magnetite nanoparticle clusters with tunable cluster size and magnetic field sensitivity	Dalton Trans.	40	1073-1078	2011

V. Singh, S. Takami, K. Minami, D. Hojo, T. Arita, T. Adschiri	Hybridisation of Sebaic Acid onto the Surface of gamma-Alumina Nanoparticles in Sub- and Supercritical Water	Z. Naturforsch., B: Chem. Sci.	65b	1045-1050	2010
B. Shahmoradi; I. A. Ibrahim; N. Sakamoto; S. Ananda; T.N. Guru Row; Kohei Soga; K. Byrappa; S. Parsons; Yoshihisa Shimizu	In situ surface modification of molybdenum-doped organic?inorganic hybrid TiO2 nanoparticles under hydrothermal conditions and treatment of pharmaceutical effluent	,ENVIRONMENTAL TECHNOLOGY	31	1213-1220.	2010
Kohei Soga, Kimikazu Tokuzen, Kosuke Tsuji, Tomoyoshi Yamano, Hiroshi Hyodo and Hidehiro Kishimoto	NIR Bioimaging: Development of Liposome-Encapsulated, Rare-Earth-Doped Y2O3 Nanoparticles as Fluorescent Probes	EUROPEAN JOURNAL OF INORGANIC CHEMISTRY	2010	2673-2677.	2010
T. Zako, H. Hyodo, K. Tsuji, K. Tokuzen, H. Kishimoto, M. Ito, K. Kaneko, M. Maeda and K. Soga	Development of Near Infrared-Fluorescent Nanophosphors and Applications for Cancer Diagnosis and Therapy	JOURNAL OF NANOMATERIALS	2010	1-8	2010
K. Soga and Y. Nagasaki	Polyscale technology for developing near infrared fluorescence bioimaging system based on novel synthese approaches for rare-earth doped nanophosphors	MATERIALS RESEARCH INNOVATIONS	14	51-55	2010

C. K. Chandrashenkar, B. Basavalingu, K. M. Lokantha Rai, S. Ananda, T. Tonthai, K. Soga and K. Byrappa	Novel method of synthesis of R3+:YVO4 (where R=Nd, Er) crystals	MATERIALS RESEARCH INNOVATIONS	14	38-44	2010
Takanari Togashi	One-pot Hydrothermal Synthesis of an Assembly of Magnetite Nanoneedles on a Scaffold of Cyclic-diphenylalanine Nanorods	Journal of Nanoparticle Research		in press	2011
Do-Myoung Kim, Mitsuo Umetsu, Kyo Takai, Takashi Matsuyama, Nobuhiro Ishida, Haruo Takahashi, Ryutaro Asano, and Izumi Kumagai	Enhancement of cellulolytic enzyme activity by clustering of cellulose binding domain on nanoscaffolds	Small	7	656-664	2011
Takanari Togashi, Nozomi Yokoo, Mitsuo Umetsu, Satoshi Ohara, Takashi Naka, Seiichi Takami, Hiroya Abe, Izumi Kumagai, and Tadafumi Adschiri	Material-binding peptide application -ZnO crystal structure control by means of a ZnO-binding peptide	Journal of Bioscience and Bioengineering	11	140-145	2011
Mitsuo Umetsu, Takeshi Nakanishi, Ryutaro Asano, Takamitsu Hattori, and Izumi Kumagai	Protein-protein interactions and selection: generation of molecule-binding proteins on the basis of tertiary structural information	FEBS Journal	277	2006-2014	2010

MedChemComm

www.rsc.org/medchemcomm

Volume 1 | Number 3 | September 2010 | Pages 173–240

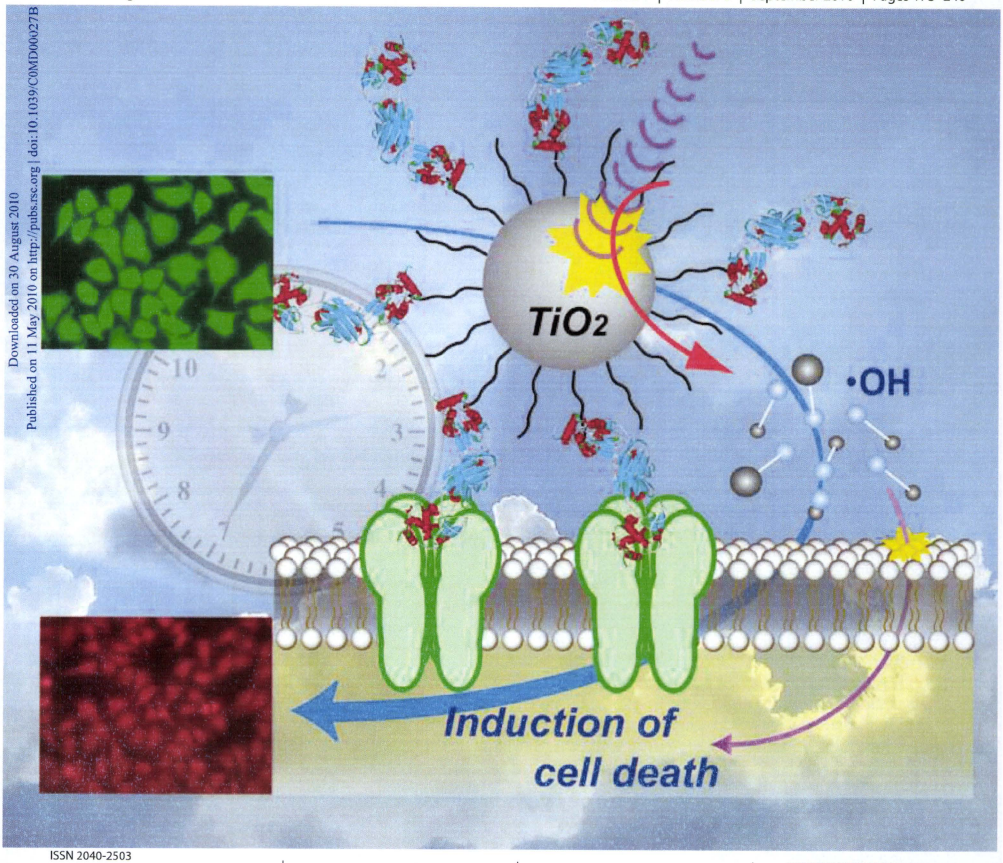

ISSN 2040-2503

RSC Publishing

EFMC
European Federation
for Medicinal Chemistry

CONCISE ARTICLE
Chiaki Ogino *et al.*
Biofunctional TiO_2 nanoparticle-mediated photokilling of cancer cells using UV irradiation

2040-2503(2010)1:3;1-W

Biofunctional TiO_2 nanoparticle-mediated photokilling of cancer cells using UV irradiation†

Kazusa Matsui,[a] Miki Karasaki,[a] Maiko Segawa,[a] Sang Youn Hwang,[b] Tsutomu Tanaka,[b] Chiaki Ogino*[a] and Akihiko Kondo[a]

Received 12th March 2010, Accepted 2nd April 2010
DOI: 10.1039/c0md00027b

Cancer cell-specific photokilling was successfully demonstrated using antibody-immobilized TiO_2 nanoparticles with only 1 J cm^{-2} UV irradiation.

Introduction

In the context of cancer therapy, nanoparticles (NPs) such as platinum,[1] gold,[2] quantum dots and liposomes have attracted great interest.[3] Compared with organic nanoparticles such as liposomes or chitosan, metal nanoparticles have the advantage that due to their photodynamic characteristics, their therapeutic effect is autonomous and, thus, does not require encapsulation of therapeutic agents. Among various metal nanoparticles, titanium dioxide (TiO_2) has a great generation property of reactive oxygen species (ROS) under ultraviolet (UV) light excitation depending on the sizes and morphologies of the particles.[4] In spite of its high potential for photodynamic cancer therapy (PDT), the use of these particles has been hampered because of the difficulty of size control, aggregation in aqueous solution and nanotoxicity itself[5,6], and so far only studies on their antibacterial effect have been successful.[7] Few studies on cancer cell-specific photokilling by TiO_2 are reported;[8] however, they only focus on the immobilization method of the biomolecule or mechanical delivery method. To control this "friends and foes" photocharacteristic of TiO_2 under UV irradiation, a fundamental study about the relationship between TiO_2 concentration and UV irradiation strength is necessary. In addition, cancer cell-specific molecules have to be immobilized to reduce the side effect on normal cells around the cancer.

In this study, to expand the versatility of TiO_2 NP-mediated cell-specific photokilling method, we evaluated the cytotoxicity of TiO_2 NPs according to UV irradiation strength, and measured photokilling of target cells *via* active cell targeting using antibody-immobilized TiO_2 NPs.

Experimental

Preparation of antibody-immobilized TiO_2 nanoparticles

Two kinds of TiO_2 NPs were used in this study, with sizes of about 30 nm and 10 nm, as measured by dynamic light scattering. For surface modification of TiO_2 NPs, polyacrylic acids (PAA) were used to avoid TiO_2 NP aggregation under physiological conditions. PAA modification of each of the TiO_2 NPs was carried out according to previous reports.[9] UV-driven hydroxyl radical generation from various concentrations of NPs was measured using aminophenyl fluorescein (APF), which has a fluorescent response to various ROS. Chemical modifications of biofunctional molecules on the PAA-modified TiO_2 NPs were made with *N*-hydroxysuccinimide and 1-ethyl-3-(3-dimethylaminopropyl) carbodiimide hydrochloride chemistries.[9] The variable domain of a camelid heavy chain-only antibody (la), which has high affinity to EGFR and is prepared easily using *Escherichia coli* as a host,[11] was immobilized as a cell-specific homing molecule on TiO_2 NPs. Detailed experimental procedures are shown in ESI.†

Preparation and evaluation of antibody-immobilized TiO_2 nanoparticles

HeLa cells were incubated with 0.03 wt% PAA-TiO_2/la for 10 min and then directly irradiated with UV (3 J cm^{-2} or 1 J cm^{-2}). Cell toxicity was evaluated immediately or 24 h later using calcein-AM (live cells) and ethidium homodimer-1 (EthD-1, dead cells) fluorescent dye. Detailed experimental procedure are shown in ESI.†

Results and discussion

Evaluation of antibody-immobilized TiO_2 nanoparticles

Our strategy is shown in Fig. 1. First, we investigated the radical generation ability of TiO_2 and PAA-modified TiO_2 NPs with UV irradiation using fluorescence derived from APF as an indicator. TiO_2 NPs (30 nm) generated the highest fluorescence level when 0.3 and 0.03 wt% NPs were irradiated with 1.5 J cm^{-2} (Fig. 2A),

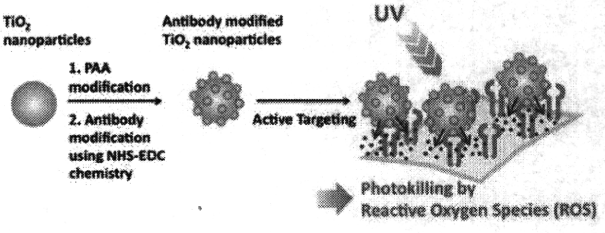

Fig. 1 Schematic illustration of target cell photokilling using antibody-modified TiO_2 nanoparticles with UV irradiation.

[a]*Department of Chemical Science and Engineering, Graduate School of Engineering, Kobe University, 1-1 Rokkodaicho, Nada-ku, Kobe, 657-8501, Japan. E-mail: ochiaki@port.kobe-u.ac.jp; Fax: +81-78-803-6193; Tel: +81-78-803-6193*
[b]*Organization of Advanced Science and Technology, Kobe University, 1-1 Rokkodaicho, Nada-ku, Kobe, 657-8501, Japan*

† Electronic supplementary information (ESI) available: Detailed experimental procedure, and Figure S1 and S2. See DOI: 10.1039/c0md00027b

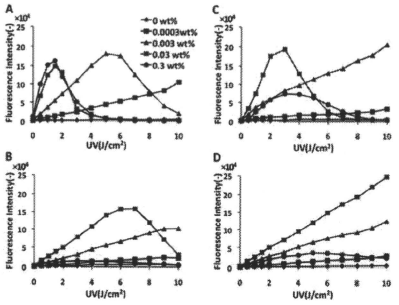

Fig. 2 The amount of radicals from TiO_2 exposed to UV. (A) TiO_2 (30 nm). (B) TiO_2 (10 nm). (C) PAA-TiO_2 (30 nm). (D) PAA-TiO_2 (10 nm).

suggesting the appropriate conditions to generate high amount of radicals. Interestingly, the fluorescence intensity decreased at higher levels of UV exposure. For NPs of lower concentration (0.003 wt%), more UV exposure (5 J cm^{-2}) was required to generate nearly the same fluorescence levels. After PAA modification, the highest fluorescence intensity was detected with 3 J cm^{-2} of exposure with 0.03 wt% NPs (Fig. 2C). We found that UV irradiation and pH did not affect APF fluorescence. PAA modification slightly decreased the amount of generated radicals, because produced radicals or UV radiation may be blocked by PAA. Similar results were obtained for TiO_2 NPs of 10 nm, although lower fluorescence (*i.e.* a smaller amount of radicals) was observed (Fig. 2B). However, after PAA modification, the amount of radicals decreased, and a maximum peak was not reached even after UV irradiation up to 10 J cm^{-2} (Fig. 2D). From these results, there was an optimal size for NPs for ROS generation with UV irradiation. TiO_2 NPs of 30 nm possessed better ROS generation potential whether the NPs were modified or not, which corresponds to a previous report.[12] For target cell-specific photokilling, a large amount of radicals should be produced with a lower NP concentration and with lower UV exposure levels. We assumed that PAA-modified TiO_2 NPs of 30 nm (hereafter named PAA-TiO_2) were optimal for protein modification and cell photokilling in further experiments.

We modified PAA-TiO_2 by anti-epidermal growth factor receptor (EGFR) antibody because EGFR is over-expressed on the surface of 20–30% of cancer cell lines.[10] The anti-EGFR antibody modification of TiO_2 NPs, named as PAA-TiO_2/la, was analyzed by SDS-PAGE. The band corresponding to PAA-TiO_2/la was observed at a much higher molecular weight, suggesting successful modification (ESI, Fig. S1†). We also confirmed the antigen-binding ability of PAA-TiO_2/la by ELISA (ESI, Fig. S2†). Anti-EGFR antibody (la) and PAA-TiO_2/la efficiently bound the HeLa cells, although PAA-TiO_2 did not bind the cell.

Cell-specific photokilling using antibody-immobilized TiO_2 NPs with UV irradiation

Encouraged by these findings, we next carried out cell-specific photokilling using PAA-TiO_2/la. HeLa cells were employed as a model of EGFR-expressing cells. The addition of PAA-TiO_2 and/or anti-EGFR antibody without UV exposure did not affect cell viability (Fig. 3, left column), suggesting low toxicity of TiO_2 NPs itself on cultured cells at this concentration. HeLa cells treated with PAA-TiO_2/la showed extensive cell death (about 50% estimated by cell counting) after UV irradiation (Fig. 3D). In contrast, there was no cell death after treatment with only PAA-TiO_2 and anti-EGFR antibody mixtures (Fig. 3B, C), or BSA-modified TiO_2 NPs after UV exposure (Fig. 3E, F). When MCF-7, which is a low EGFR expression cell line, was treated with PAA-TiO_2/la, cell toxicity was not observed even under UV exposure (Fig. 3G, H). This clearly shows that PAA-TiO_2/la NPs allow EGFR expressing cell-specific TiO_2 NP accumulation and cell-specific killing by radicals generated with UV irradiation. However, after further cultivation for 24 h following UV irradiation (3 J cm^{-2}), cells without TiO_2 NPs were detected to be dead in the end. It suggests apoptosis might be induced with large amount of UV irradiation. Therefore, to optimize the UV irradiation level, we applied UV irradiation at 1 J cm^{-2} followed by a further 24 h incubation, and then cell viability was evaluated. HeLa cells treated with PAA-TiO_2/la under UV exposure (1 J cm^{-2}) showed major cell death after 24 h incubation (Fig. 4D). In contrast, only a few dead cells under other conditions were observed (Fig. 4A–C). We also evaluated cell death depending on the amount of TiO_2 NPs with 1 J cm^{-2} UV exposure. HeLa cells were efficiently damaged (about 80% estimated by cell counting) with 0.03 and 0.003 wt% PAA-TiO_2/la (Fig. 4B, C), suggesting

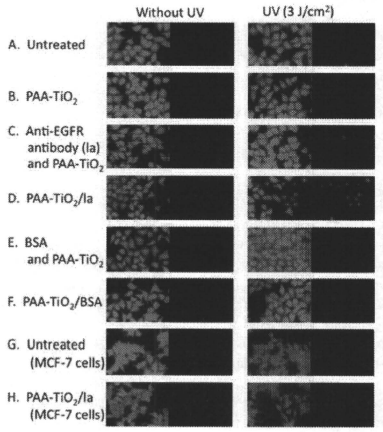

Fig. 3 HeLa cell viability after treatment with *anti*-EGFR antibody-immobilized TiO_2 NPs followed by UV irradiation (3 J cm^{-2}). Cell viability was examined immediately after UV irradiation by calcein AM/EthD-1 fluorescence staining, and representative images from each sample are shown. Cells with green fluorescence are considered alive, whereas those with red are considered dead. (A) Untreated (B) PAA-TiO_2 (C) *anti*-EGFR antibody (la) and PAATiO_2 mixtures. (D) PAA-TiO_2/la. (E) la and BSA mixture; (F) PAA-TiO_2/BSA (G) Untreated MCF-7 cells (H) MCF-7 cells treated with PAA-TiO_2/la.

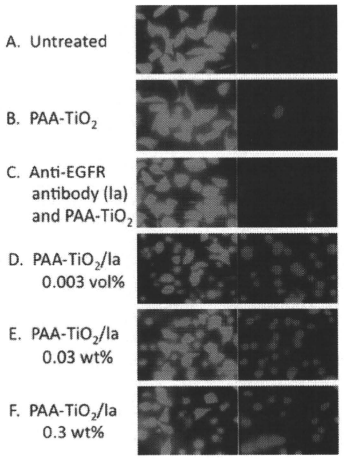

Fig. 4 HeLa cell viability after treatment with PAA-TiO_2/Ia followed by UV irradiation (1 J cm^{-2}) and further incubation for 24 h. (A) Untreated (B) PAA-TiO_2 (C) *anti*-EGFR antibody (Ia) and PAATiO_2 mixtures. (D) 0.003 wt% of PAA-TiO_2/Ia. (E) 0.03 wt% of PAA-TiO_2/Ia. (F) 0.3 wt% of PAA-TiO_2/Ia.

that accumulation around the cell surface enhanced cell toxicity caused by radical generation with UV exposure, even at a low TiO_2 NP concentration. Effective photokilling with a low TiO_2 concentration demonstrates the advantage of active targeting, and is also a desirable property in therapy.

Conclusions

We established a cell-specific photokilling method using antibody immobilized TiO_2 NPs. It allows target cell-specific killing with low TiO_2 concentrations and low UV exposure levels. Our strategy is applicable for other targeting molecules such as various antibodies or bioactive ligands, as well as photoactivating nanoparticles. Although our system can be applicable for tumors near the skin surface, one possible disadvantage is that UV irradiation cannot be exposed to deeper tissues such as the liver and pancreas. Hence, novel nanoparticles which generate ROS with some radial ray, such as X-rays or gamma-rays, should be developed in the future.

Acknowledgements

This research was supported in part by Special Coordination Funds for Promoting Science and Technology, Creation of Innovation Centers for Advanced Interdisciplinary Research Areas (Innovative Bioproduction Kobe), MEXT, Japan.

Notes and references

1 N. G. Blanco, C. R. Maldonado and J. C. Marreque-Rivas, *Chem. Commun.*, 2009, 5257–5259.
2 Y. T. Lim, M. Y. Cho, B. S. Choi, J. M. Lee and B. H. Chung, *Chem. Commun.*, 2008, 4930–4932.
3 (*a*) D. J. Bharali, M. Khalil, M. Gurbuz, T. M. Simon and S. A. Mousa, *Nanomedicine*, 2009, **4**, 1–7; (*b*) M. Ferrari, *Nat. Rev. Cancer*, 2005, **5**, 161–171; (*c*) M. E. Davis, Z. G. Chen and D. M. Shin, *Nat. Rev. Drug Discovery*, 2008, **7**, 771–782; (*d*) D. Peer, J. M. Karp, S. Hong, O. C. Farokhzad, R. Margalit and R. Langer, *Nat. Nanotechnol.*, 2007, **2**, 751–760; (*e*) N. G. Blanco, C. R. Maldonado and J. C. Mareque-Rivas, *Chem. Commun.*, 2009, 5257–5259.
4 (*a*) U. M. K. Shahed, Al-S. Mofareh and B. I. William Jr., *Science*, 2002, **297**, 2243–2245; (*b*) R. Huang, A. Wallqvist and D. G. Covell, *Biochem. Pharmacol.*, 2005, **69**, 1009–1039; (*c*) R. Cai, Y. Kubota, T. Shuin, H. Sakai, K. Hashimoto and A. Fujishima, *Cancer Res*, 1992, **52**, 2346–2348; (*d*) Y. Kubota, T. Shuin, C. Kawasaki, M. Hosaka, H. Kitamura, R. Cai, H. Sakai, K. Hashimoto and A. Fujishima, *Br. J. Cancer*, 1994, **70**, 1107–1111; (*e*) J. W. Seo, H. Chung, M. Kim, J. Lee, I. Choi and J. Cheon, *Small*, 2007, **3**, 850–853; (*f*) N. K. Shrestha, J. M. Macak, F. Schmidt-Stein, R. Hahn, C. T. Mierke, B. Fabry and P. Schmuki, *Angew. Chem., Int. Ed.*, 2009, **48**, 969–972; (*g*) Y. Luo, Y. Tian and Q. Rui, *Chem. Commun.*, 2009, 3014–6.
5 (*a*) A. Nel, T. Xia, L. Mädler and N. Li, *Science*, 2006, **311**, 622–627; (*b*) T. Xia, M. Kovochich, J. Brant, M. Hotze, J. Sempf, T. Oberley, C. Sioutas, J. I. Yeh, M. R. Wiesner and A. E. Nel, *Nano Lett.*, 2006, **6**, 1794–1807; (*c*) S. Singh, T. Shi, R. Duffin, C. Albrecht, D. van Berlo, D. Hoehr, B. Fubini, G. Martra, I. Fenoglio, P. J. A. Borm and R. P. F. Schins, *Toxicol. Appl. Pharmacol.*, 2007, **222**, 141–151.
6 S. M. Hussain, K. L. Hess, J. M. Gearhart and K. T. Geiss, *Toxicol. in Vitro*, 2005, **19**, 975–983.
7 (*a*) F. R. Marciano, D. A. Lima-Oliveira, N. S. Da-Silva, A. V. Diniz, E. J. Corat and V. J. Trava-Airoldi, *J. Colloid Interface Sci.*, 2009, **340**, 87–92; (*b*) D. S. Kim and S. Y Kwak, *Environ. Sci. Technol.*, 2009, **43**, 148–151; (*c*) B. K. Erdural, A. Yurum, U. Bakir and G. Karakas, *J. Nanosci. Nanotechnol.*, 2008, **8**, 878–886; (*d*) C. Hu, J. Guo, J. Qu and X. Hu, *Langmuir*, 2007, **23**, 4982–4987.
8 (*a*) A. R. Elena, U. Ilya, L. Barry, M. D. Nada, S. L. Maciej and R. Tijana, *Nano Lett.*, 2009, **9**, 3337–3342; (*b*) J. Xu, Y. Sun, J. Huang, C. Chen, G. Liu, Y. Jiang, Y. Zhao and Z. Jiang, *Bioelectrochemistry*, 2007, **71**, 217–222.
9 (*a*) K. Kanehira, T. Banzai, C. Ogino, N. Shimizu, Y. Kubota and S. Sonezaki, *Colloids Surf., B*, 2008, **64**, 10–15; (*b*) C. Ogino, K. Kanehira, R. Sasai, S. Sonezaki and N. Shimizu, *J. Biosci. Bioeng.*, 2007, **104**, 339–342.
10 (*a*) N. E. Hynes and D. F. Stern, *Biochim. Biophys. Acta*, 1994, **1198**, 165–184; (*b*) V. P. Collins, *Semin. Cancer Biol*, 1993, **4**, 27–32.
11 R. C. Roovers, T. Laeremans, L. Huang, S. De Taeye, A. J. Verkleij, H. Revets, H. J. de Haard and P. M. P. van Bergen en Henegouwen, *Cancer Immunol. Immunother.*, 2007, **56**, 303–317.
12 J. Jiang, G. Oberdoumlrster, A. Elder, R. Gelein, P. Mercer and P. Biswas, *Nanotoxicology*, 2008, **2**, 33–42.

Published online 2 December 2009

Nucleic Acids Research, 2010, Vol. 38, No. 4 ***e21***
doi:10.1093/nar/gkp1101

Selection of DNA aptamers using atomic force microscopy

Yusuke Miyachi[1], Nobuaki Shimizu[2], Chiaki Ogino[1,*] and Akihiko Kondo[1]

[1]Department of Chemical Science and Engineering Faculty of Engineering, Graduate School of Engineering, Kobe University, Rokkoudai-chou 1-1, Nada, Kobe 657-8501 and [2]Division of Material Sciences, Graduate School of Natural Science and Technology, Kanazawa University, Japan

Received August 10, 2009; Revised October 23, 2009; Accepted November 9, 2009

ABSTRACT

Atomic force microscopy (AFM) can detect the adhesion or affinity force between a sample surface and cantilever, dynamically. This feature is useful as a method for the selection of aptamers that bind to their targets with very high affinity. Therefore, we propose the Systematic Evolution of Ligands by an EXponential enrichment (SELEX) method using AFM to obtain aptamers that have a strong affinity for target molecules. In this study, thrombin was chosen as the target molecule, and an 'AFM-SELEX' cycle was performed. As a result, selected cycles were completed with only three rounds, and many of the obtained aptamers had a higher affinity to thrombin than the conventional thrombin aptamer. Moreover, one type of obtained aptamer had a high affinity to thrombin as well as the anti-thrombin antibody. AFM-SELEX is, therefore, considered to be an available method for the selection of DNA aptamers that have a high affinity for their target molecules.

INTRODUCTION

Aptamers are rare functional nucleic acid motifs derived from libraries of nucleic acids by iterative rounds of selection and amplification using a process called Systematic Evolution of Ligands by EXponential enrichment (SELEX) (1–5). In the aptamer selection process, the oligonucleotide library is incubated with a target of interest and a buffer of choice at a given temperature. The bound oligonucleotides are then separated from the unbound oligonucleotides, either by filtration on nitrocellulose filters or by affinity processes such as covalent binding to a titer plate or streptavidin (SA)-coated beads. Aptamers have been selected for a wide variety of targets—for example, low-molecular compounds such as ethanolamine ATP (5–13) and proteins (14–17). Importantly, the isolated aptamers often show high specificity and affinity to their cognate targets. These properties expand the possible applications of aptamers, including their use in diagnosis (13,18–20), therapy and imaging processes (21,22).

Previously reported methods for aptamer selection have included affinity chromatography separation step (14–17). The successful selection of high-affinity aptamers from a library of nucleic acids depends mainly on the efficiency with which the unbound species can be separated from the bound sequences. In many cases, however, DNA aptamers selected by conventional SELEX strategy for adenosine triphosphate (K_D: 1×10^{-6} order), hematoporphyrin (K_D: 1×10^{-4} to 1×10^{-6}) and thrombin (K_D: 1×10^{-7} order), have a low affinity (7–17). Since the dissociation constant of antibody, often used for biosensing device, had been reported to be 1×10^{-8} to 1×10^{-10} M, the affinities of these reported DNA aptamers were weaker than that of antibody to antigen (23–27). When DNA aptamers are used with biosensing devices, a low affinity to the target molecule will result in unreliable results for detection sensitivity.

Atomic force microscopy (AFM) is a method that scans the imperceptible sample surface using a probe called a cantilever, detecting the weak force between sample surface and probe, and makes pictures of the sample surface. AFM can also dynamically detect the adhesion or affinity force between the sample surface and the cantilever (21,22,28,29). This notable feature is useful for measurement of the affinity force of biomolecule interactions using the biomolecule immobilized cantilever and the sample. This system is considered to be a selection method for aptamers. Therefore, we propose the SELEX method using AFM to obtain aptamers having a strong affinity to target molecules.

The selection scheme of this SELEX strategy is shown in Figure 1. DNA aptamers with a very strong affinity to target molecules were obtained by repeating this cycle. In this study, thrombin was chosen as the target molecule of the DNA aptamer, and the selection cycles were repeated for three rounds. As a result, the obtained DNA aptamers had a high affinity to thrombin than that

*To whom correspondence should be addressed. Tel/Fax: +81 78 803 6193; Email: ochiaki@port.kobe-u.ac.jp

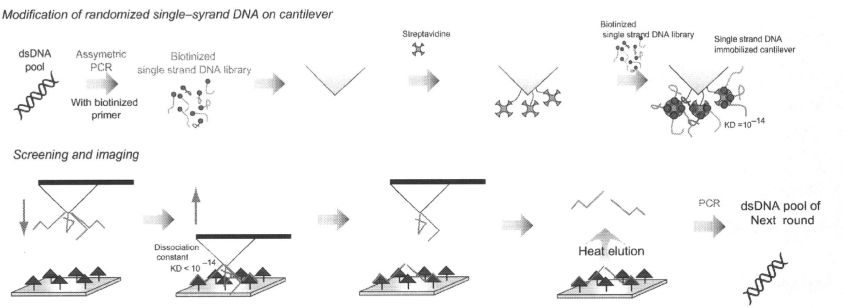

Figure 1. The scheme of a new SELEX strategy for functional oligonucleotide screening by AFM.

of conventional thrombin aptamer. One type of DNA aptamer exhibited high affinity as well as that of an antibody.

MATERIALS AND METHODS

Materials

Thrombin from human plasma and streptavidin from *Streptomyces avidinii* were purchased from Sigma (MO, USA). Anti-human thrombin antibody from sheep was purchased from Funakoshi (Tokyo, Japan). DNA polymerase was purchased from Roche Diagnostics (Basel, Switzerland). A microspin column was purchased from GE Healthcare (MO, USA). 3,3′-Dithiobis [sulfosuccinimidylpropionate] (DTSSP) was purchased from Pierce (MO, USA). The other chemicals used were analytical grade and were purchased from Nacalai Tesque (Kyoto, Japan).

Preparation of the cantilever as modified by single-strand DNA (ssDNA) library

In the primary round, for double-strand DNA library (dsDNA) production, a synthetic DNA oligonucleotide library (104-mer) with 60 random nucleotide sequences, 5′-TAGGGAATTCGTCGACGGATCC-N60-CTGCAG GTCGACGCATGCGCCG-3′, was amplified over 25 cycles of PCR (95°C, 15 s; 72°C, 30 s) using the following pair of primers: 5′-TAATACGACTCACTATAGGGAA TTCGTCGACGGAT-3′ (P1) and 5′-CGGCGCATGCG TCGACCTG-3′ (P2). The ssDNA library was then obtained from the dsDNA by an additional 90 cycles of asymmetric PCR using 5′ biothinated P1 primer. The PCR product, ssDNA, was purified by microspin column.

To clear away the organic compounds that adhered on the cantilever, the cantilever was treated with UV for 2 h. The probe was then exposed to 100 µl of 2 mg/ml DTSSP solution in 20 mM acetate (pH 4.8) at room temperature for 30 min. After the reaction, the probe was dipped in 20 ml of ultra pure water to remove unreacted DTSSP. The succinimide immobilized probe was then doused at room temperature for 1 h with 100 µl of 1 mg/ml streptavidin solution in PBS, followed by washing with 20 ml of folding buffer. After immobilization of streptavidin on the cantilever, 100 µl of 5 µM biothinated ssDNA was dropped on the cantilever and incubated at room temperature for 30 min. Finally, the ssDNA immobilized probe was put in 20 ml of folding buffer containing 0.01% Tween 20 to remove unbound biothinated ssDNA.

Preparation of gold chip modified by thrombin

A gold chip was covered by 200 µl of 4 mg/ml DTSSP solution in 20 mM acetate at room temperature for 30 min. The chip was then washed with 10 ml of ultra pure water. After washing, the succinimide immobilized gold chip was covered with 200 µl of 6 µg/ml thrombin solution in PBS at room temperature for 1 h. Finally, the gold chip was washed with 10 ml of folding buffer.

SELEX strategy based on AFM

Force curve mapping was performed in the liquid cell of a SPA400-Nanonavi AFM unit (SII Nanotechnology Inc., Chiba, Japan) with the cantilever and gold chip described above. The force curve measurements were performed in folding buffer [50 mM Tris–HCl (pH 7.6), 300 mM NaCl, 30 mM KCl and 5 mM $MgCl_2$]. Force curves were recorded at a velocity of 17 µm/s. Topographic images were captured at 64 × 64 pixels resolution with a scan size of 1 µm × 1 µm. The adhesion forces analysis between ssDNA immobilized on tip of cantilever and thrombin were measured at 4096 data points (64 × 64 point), and a histogram of these adhesion force was charted. According to the AFM-SELEX, scanning was carried out five times (4096 × 5 times) in round 1 and 2, and 4 times (4096 × 4 times) in round 3, respectively.

After the scanning and force curve mapping, the ssDNA-bound gold chip was washed with 10 ml folding

buffer containing 0.01% Tween 20. Then, to elute ssDNA on the gold chip, the chip was dunked in 2 ml of 20 mM TE buffer containing 1% DMSO and incubated at 98°C for 10 min and on ice for 10 min. The eluted ssDNAs were precipitated by ethanol, dissolved in 100 µl of 20 mM TE buffer, and used for the next selection as a PCR template.

Cloning and sequencing

The dsDNAs obtained after the fourth rounds of selection were subcloned into pT7 blue vector, and then transformed into *Escherichia coli* (Nova blue). The plasmid DNA was isolated by the alkaline-extraction method. Twenty-two colonies were randomly selected after the fourth round, and these DNA sequences were determined by a dye-terminator method using CEQ 8000 (Beckman).

Affinity assay of obtained aptamers by AFM

For dsDNA production, obtained DNA was amplified over 15 cycles of PCR (95°C, 15 s; 72°C, 30 s) using P1 and P2 primer. The ssDNA was then obtained from the dsDNA by an additional 90 cycles of asymmetric PCR using 5′ biothinated P1 primer. The PCR product, ssDNA, was purified by microspin column.

The preparation of the cantilever immobilizing ssDNA and the gold chip immobilizing thrombin was followed by selection methods. The affinity force of the conventional thrombin aptamer and antibody to thrombin was analyzed as a positive control under the same conditions.

Fluorescence polarization measurement

The dissociation constant of TBA-1 was calculated by fluorescence polarization. Each of various concentrations of thrombin and FITC labeled TBA-1 (final concentration: 100 nM) was mixed in the folding buffer for 2 h, and fluorescence polarization measurement was carried out (EnVision, Perkin elmer, Wellesley, MA). As a negative control of thrombin, 100 nM streptavidin was used, and fluorescence polarization measurement was carried out under same condition. Each data was represented three independent experimental data, and each error bar was mean of standard deviation.

RESULTS

Selection of DNA aptamer using AFM

At first, the biotinated random ssDNA was immobilized on the cantilever through avidin, and the target molecules were immobilized on the gold chip. The prepared cantilever and gold chip were simultaneously applied to AFM as a DNA-modified probe and thrombin immobilized chip, respectively. When the cantilever approached the gold chip, the DNA aptamer that binds the target molecules would bind the target immobilized on the gold chip. If the affinity force with target is very strong, the avidin-biotin interaction is fractured, and DNA aptamer remains on the gold chip. The remaining DNA was recovered by heat elution amplified by PCR.

The selection cycle by AFM-SELEX was repeated for three rounds. The histogram of the affinity force between ssDNA and thrombin was developed from 4096 force curves from each round (Figure 2A–D). As a result, the affinity force between ssDNA and thrombin was gradually increased with repeated selection rounds. The initial ssDNA and round 1 elution pool had low affinity force to thrombin (Figure 2A and B). However, in the round 2 elution pool the force was higher, over 100 pN, and in the round 3 elution pool the histogram of affinity force had a peak at 320–329 pN. Using the histogram data, the average affinity force of each round was calculated (Figure 2E). The average force of the initial pool was ~57.15 pN (Figure 2A and E). However, after only three repeated rounds of the AFM-SELEX method, the ssDNA pool had 411.52 pN of strong affinity to thrombin (Figure 2D and E).

In Figure 3, the topography of the affinity force between the round 3 elution pool and thrombin is shown. The highest point of affinity force was concentrated late in the scanning (Figure 3A). Moreover, the force had no relationship with the roughness of the sample, since the higher force was not operating at the height of the surface roughness.

Cloning and sequencing

The dsDNAs obtained after the third round of selection were subcloned into pT7 blue vector. Twenty-two colonies were randomly selected, and these DNA sequences were determined (Table 1). Many of the obtained DNAs had G-rich sequences. The sequence called TBA-1 had the largest share of obtained aptamers. Moreover, the sequences of TBA-1 and -2 had many 'GGGGT' motifs.

Binding assay using AFM

The immobilization method described above was followed by the SELEX protocol. The prepared cantilever and gold chip were applied to AFM to analyze the affinity force between ssDNA and thrombin. The resulting force histogram of TBA-1 had one peak at 210-219 pN (Figure 4A). The histogram of TBA-2 had two peaks at 40–49 and 110–119 (Figure 4B). The average affinity force between thrombin and the obtained aptamers was calculated. The obtained aptamers had a higher affinity for thrombin than N60 ssDNA and the conventional thrombin aptamer (Figure 4C and Table 2). TBA-1 had the highest affinity of the obtained DNA aptamers. The affinity force of the conventional DNA aptamer that has the 'GGTTGGTGT GGTTGG' sequence was also measured by AFM, and the resulting force average was 65.09 pN. The average affinity force was 205.52 pN, and the value was about three times higher than that of the conventional thrombin aptamer. The affinity force between anti-thrombin antibody and thrombin was then analyzed by AFM. The resulting average affinity force was 91.59 pN (Figure 4D and Table 2).

Fluorescence polarization measurement

The fluorescence polarization measurement between TBA-1 and thrombin was carried out, and the recognition affinity obtained by AFM analysis was re-confirmed.

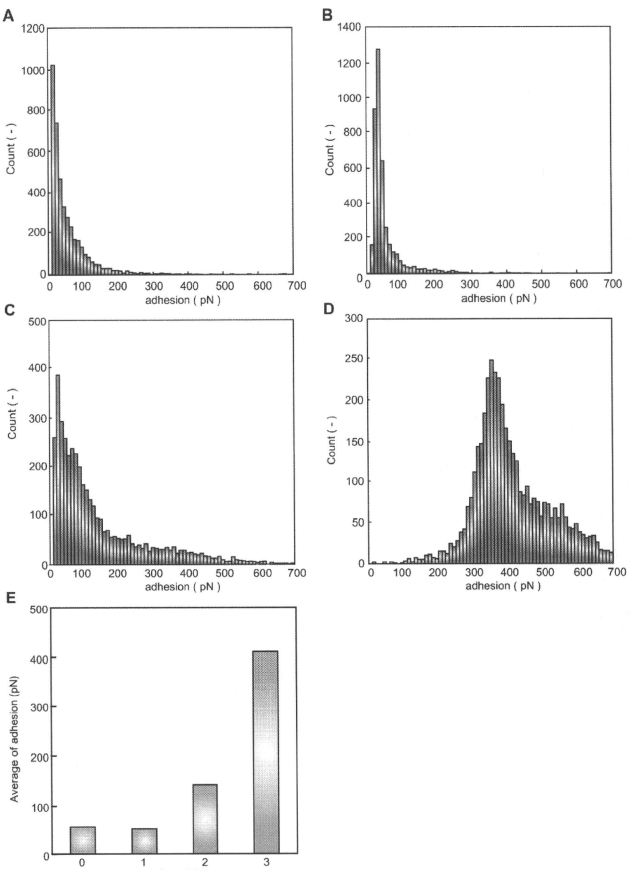

Figure 2. Histogram of adhesion force between ssDNA and protein for 4096 data points. (**A**) adhesion force between 0 pool ssDNA and thrombin, (**B**) adhesion force between round 1 elution pool and thrombin, (**C**) adhesion force between round 2 elution pool and thrombin, (**D**) adhesion force between round 3 elution pool and thrombin and (**E**) the average of affinity force between each round elution pool and thrombin.

The concentration of thrombin was changed from 10^{-13}–10^{-7} M, and then polarization value was plotted against the concentration of thrombin (Figure 5). As a result, the fluorescence polarization value was increased with concentration dependency. On the other hand, polarization value of FITC-labeled TBA-1 against with 100 nM streptavidin was not increased significantly (Table 3).

DISCUSSION

SELEX strategy using AFM

The selection of a DNA aptamer with AFM was performed using 60 random nucleotide sequences. After the first SELEX round, dsDNA was not amplified enough by 15 PCR cycles, since the amount of elution DNA was very

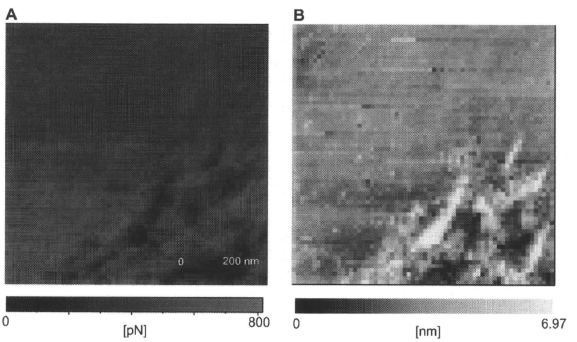

Figure 3. Affinity image between round 3 elution pool and thrombin showing the affinity images (**A**) as well as the topography images (**B**).

Table 1. Sequence of obtained single-strand DNA

Sequence name	Sequence of random region	Count
TBA1	CCTAGTGTGCGTCGATGGGGTGGGGTGGGGCTGAGTTGGGGGGTGGGATCAATCAATCTGGTTT	8
TBA2	CCTAGTGTGCGTCGATGGGGTGGGGTGGGGCTGAGTTGGGGGGTGGGATCAATCCATCTGGTCT	2
The other 1	CCCACGGAGTCACCATTGATCACAACCCCAGCT	1
The other 2	CCCACGGAGCCACCACCTTGATCACAACCCTCAGCT	1
The other 3	CCCACGGAGTCACCCTTGATCACAACCTCAGCT	2
The other 4	CCCACGGAGTCACCCTTGACCACAATCTCAGCT	1
The other 5	CCCACGGAGCCACCCTTGATCACAGCCTCAGCT	1
The other 6	CCCACGGAGTCACCCTTGATCACGAACCTCAGCT	1

small (data not shown). However, after the third SELEX round, the amount of dsDNA amplified by PCR was determined by PAGE to be large. Based on these results, selection by the AFM-SELEX strategy appeared to be very strong, and the ssDNA that binded strongly to thrombin was selected.

The selection cycle was repeated for three rounds. Figure 2 shows the histogram of adhesion force between ssDNA and thrombin. The initial ssDNA pool had a low adhesion force to thrombin, since the ssDNA had a low affinity for thrombin (Figure 2A). However, when the AFM-SELEX method was repeated for three rounds, the ssDNA had a strong affinity for thrombin (Figure 2D). Moreover, the third round elution pool did not have a large adhesion force to streptavidin, ~67.14 pN (data not shown). This result shows that the third round elution pool bound specifically to thrombin. The affinity force between ssDNA and thrombin then gradually became stronger with repeated selection rounds (Figure 2E). Therefore, it is considered that ssDNA had an affinity for thrombin and was enriched by the repeating of the AFM-SELEX cycles.

In many articles on DNA aptamer, the selection cycle is repeated for more than eight rounds (8–12). However, in the selection method with AFM, the DNA aptamer with a high affinity for the target molecules was obtained by repeating only three rounds. Therefore, the AFM-SELEX strategy is a very useful method to rapidly obtain a DNA aptamer. In this new SELEX strategy using AFM, the oligonucleotide that could be bound to thrombin was only remained on gold chip. Therefore, compared with conventional SELEX strategy, it is considered that the non-specific bound of DNA was assumed to be reduced on gold chip surface, and the DNA aptamer that have high affinity to thrombin could be rapidly obtained.

The topography between round 3-elution pool and thrombin was analyzed (Figure 3B). In commonly, at the point of large roughness, the large force was occurred because of impact between cantilever and surface roughness. However, the high affinity forces, caused by molecular interaction between selected DNA aptamers and thrombin, were observed in every place, and this phenomenon was not related to the result of topology analysis (Figure 3A). Together these results, it was concluded that the specific affinity originated by molecular interaction was not related on surface roughness, and the specific adhesion force by affinity between round-3-elution pool and